Numerical Simulation of Plasma-Immersion Ion Implantation on Insulators

Christophe P. CORNET, David R. McKENZIE and Marcela M. M. BILEK

Applied and Plasma Physics, The University of Sydney, NSW, 2006, Australia.

(Received: 4 September 2008 / Accepted: 22 December 2008)

In plasma immersion ion implantation (PIII), a high voltage pulsed bias is applied to a substrate to accelerate ions from a surrounding plasma for implantation beneath the surface. This technique is often used to modify the surface properties of materials. For example, the intrinsic stress of thin films can be lowered, resulting in improved adhesion. For conducting samples, the energy of the incoming ions is directly related to the bias voltage applied. However, PIII of insulators is known to lead to a reduced bias potential due to surface charging. Previous work has attempted to measure the time-dependent charging of an insulating surface both directly and by measuring sheath collapse. In this paper, the sheath collapse near a circular insulating sample on a conducting stage is modeled by a hybrid particle-in-cell simulation. As a result of surface charging, the sheath is observed to collapse earlier at the center of the sample than at the edge. This has important implications for dose uniformity in implantation depth for insulating samples. We will present results showing the distribution of implanted ion fluence, energy and angle.

Keywords: ion implantation, cathodic arc, insulator, sheath collapse, particle-in-cell simulation.

1. Introduction

Plasma immersion ion implantation (PIII) is a method of energetic implantation of ions into a sample. The sample is placed in a plasma environment and a large negative potential, typically in the order of −kV, is applied to the sample. An ion sheath develops and the ions in the plasma are accelerated towards the sample. The energy of the impinging ions is sufficient to penetrate into the sample, changing surface properties such as thin film stress relief [1], wettability [2], wear resistance [3] and biocompatibility [4]. In recent work [5] it has been shown that PIII treatment of a polymer surface creates binding sites that enable strong attachment of proteins. When a metal plasma is used in PIII, the process is typically known as metal plasma-immersion ion implantation and deposition (MePIIID) [6].

For conducting samples, the implantation energy can be directly calculated from the applied potential. However for insulating samples, dielectric capacitance and surface charging reduce the implantation energy and the extent of surface modifications. During implantation of insulating samples, the sheath that develops around the sample has been observed to collapse [7] due to surface charging. Previous work [8] has attempted to directly measure this surface charge by measuring the voltage of a copper electrode placed on the insulator surface.

While there has been a significant amount of work that simulates PIII of conducting surfaces, there have only been a limited amount of simulation studies on PIII of insulators. One such computer simulation of PIII of insulators [9,10] has shown the importance of the role the insulator plays in the sheath dynamics and ion dose in gas-based PIII systems.

There have also been very limited studies done on ion sheath dynamics in MePIIID systems with insulators. Experiments have shown that an ion sheath collapse occurs due to surface charging of the insulator. While a simple analytical model has been developed to explain the results, computer simulation work is needed to further investigate the ion sheath collapse and its importance in ion implantation.

In this work, we develop a 2D hybrid particle in cell (PIC) model to observe the ion sheath collapse and investigate its effects.

2. Method

The simulated region of the cylindrical vacuum chamber is shown in Fig. 1. Extending from the central axis out to the chamber wall at r = 10 cm, the region of interest was 40 cm high. The sample holder was a conducting disc of diameter 7.2 cm and thickness 1.2 cm, which was supported by a conducting rod of 1 cm radius that extended 24 cm in the negative-z direction and out of the simulated region of the vacuum chamber. The top of the sample holder was 17 cm away from the top of the simulated region. The rod and sample holder were pulse biased to −20 kV. An insulating sample of dielectric constant $\varepsilon_r = 1.2$ and thickness 6 mm thickness covered the top and sides of the sample holder, the shape of the insulator has been adapted from previous experimental work on ion sheath collapse [7]. In Fig. 1, the sample is

author's e-mail: cornet@physics.usyd.edu.au

shown in light grey and the sample holder is shown as dark grey. The horizontal axis in Fig. 1 extends all the way to the edge of the vacuum chamber and the vertical axis extends from 20 to 30 cm from the bottom of the simulated region of the chamber.

A titanium plasma from a filtered cathodic arc source was injected from a 5 cm radius duct at the top of the simulated region at a drift velocity of 1.3×10^4 ms^{-1}, with an average charge state of 2.03, electron temperature, T_e, of 2.5 eV and a plasma density, n_0, of 6×10^{15} m^{-3}. These parameters closely match those of previous simulation work on Me-PIIID on conductors [11]. The operating pressure is typically at 1×10^{-4} Pa, so that the mean free path was larger than the sheath size and the effect of collisions could be ignored in this study. Other inelastic processes such as ionization and recombination were also ignored.

The plasma was modelled using a hybrid-PIC method in *r*-*z* cylindrical co-ordinates. The electrons were assumed to follow the Boltzmann relation

$$n_e = n_0 \exp\left(\frac{e\phi}{k_B T_e}\right), \tag{1}$$

where k_B is the Boltzmann's constant, e is the elementary charge and ϕ is the electrostatic potential. The ions dynamics were modeled by the PIC method [12]. The simulation domain was covered by a square lattice of cells of side length 2 mm. This value was chosen as it has been shown to be sufficiently fine to resolve the sheath features under these plasma conditions [11]. The size of the PIC particles was chosen such that the plasma density n_0 was achieved by placing 121 particles in each cell.

To solve for the electrostatic potential, the Poisson equation is written in r-z cylindrical co-ordinates

$$\nabla^2\phi = \frac{\partial^2\phi}{\partial z^2} + \frac{1}{r}\frac{\partial}{\partial r}\left(r\frac{\partial\phi}{\partial z}\right) = -\frac{e}{\varepsilon_0}\left(n_i - n_e\right). \tag{2}$$

The ion density n_i is determined from bilinear weighting of the particle to the nodes [12]. The electron density n_e, determined by the Boltzmann relation (1) was linearized [13] and the Poisson equation (2) was solved using the Gauss-Seidel relaxation method. At the earthed chamber wall (positive-*r* edge) the potential was set to zero and at the centre of the chamber ($r = 0$), L'Hôpital's rule was used to remove the singularity in the Poisson equation. At the top and bottom edges ($z = 0$ and 40 cm) Von Neumann boundary conditions were implemented, i.e. the gradient in potential in the *z*-direction was set to zero. These boundary conditions were chosen to model an open-ended cylinder. On the dielectric surface, the potential was chosen to ensure the dielectric surface condition

$$\varepsilon_r E_{in}^{\perp} - E_{out}^{\perp} = \frac{\sigma}{\varepsilon_0}, \tag{3}$$

where ε_r is the dielectric constant of the insulating material, $E_{in}^{\perp}$ and $E_{out}^{\perp}$ are the normal components of the electric field inside and outside the insulator respectively, σ is the accumulated surface charge density, and ε_0 is the permittivity of free space. Using the finite difference method, Eq. (2) can be re-written as

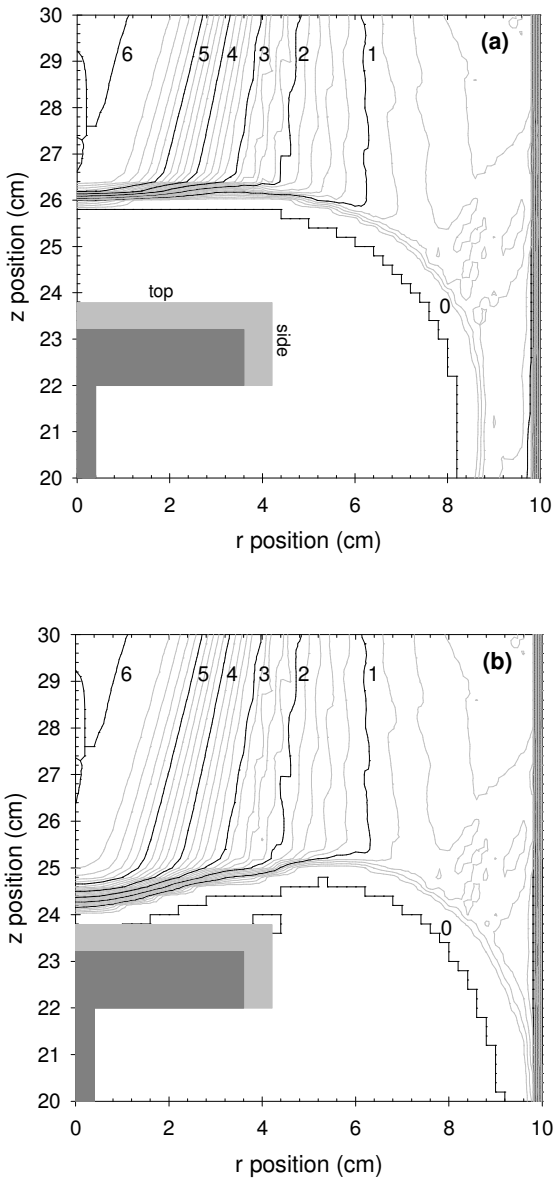

Fig.1 The electron density (a) 1 and (b) 3 μs after the pulse has been applied. The numbers denote multiples of 10^{15} m^{-3}. The dark grey represents the conducting stage and the light grey the insulating sample. It can be seen sheath collapse is faster near the centre of the stage than it is near the stage edge.

$$\phi = \frac{\varepsilon_A \phi_A + \varepsilon_B \phi_B + \sigma h}{\varepsilon_A + \varepsilon_B}, \tag{4}$$

where ϕ_A and ϕ_B are the electric potentials on the adjacent nodes in the A and B media respectively, and h is the distance between the nodes.

The surface charge was calculated from the surface ion fluence accumulated from the implanting PIC particles and an electron contribution due to electron effusion from the nearby plasma. The electron flux onto the insulator due to effusion is

$$F = \frac{n_e}{4}\sqrt{\frac{8k_B T_e}{\pi m_e}}, \tag{5}$$

where m_e is the electron mass and n_e is the electron density, which is given by the Boltzmann relation (1).

3. Results and discussion

Fig. 1(a) shows the electron density 1 μs after the pulse is applied. The convex sheath shape, which resembles the sheath surrounding a conducting sample immediately after a negative bias pulse is applied, is the *matrix sheath* in which electrons have been repelled, but ions have not yet moved. At the centre (r = 0) the sheath edge is parallel to the sample, so that ions implant normally to the surface. Further from the centre, the convex sheath deflects ion trajectories inwards and implantation becomes more oblique.

Fig 1(b) shows the electron density 3 μs after the pulse is applied. At this time, the sheath has begun to collapse. At large r, the sheath remains convex, however near r = 0, the sheath has become concave. This means that ions travelling through the sheath now get deflected outwards and the distribution of ion dose on the surface is altered.

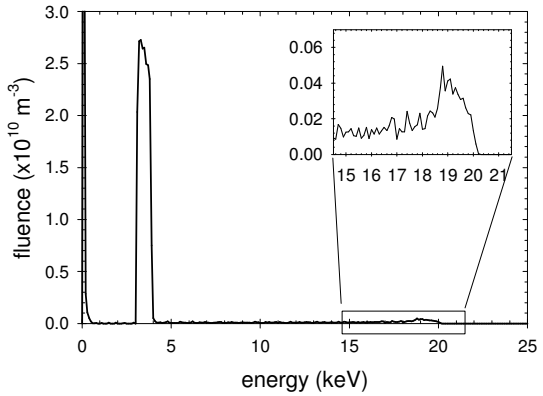

Fig.2 The accumulated ion energy distribution (IED) at a point r = 1.6 cm on the top of the insulating sample. There are clear peaks at 0 and 3.5 keV. There is also a very small tail extending to 20 keV and a small peak (insert) at 19 keV.

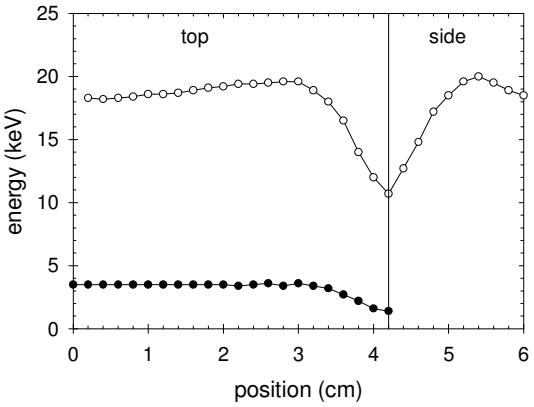

Fig.3 Peak positions in the ion energy distribution as a function of position along the sample. The higher-energy peak (open circles) has a marked decrease at the edge of the sample. The lower-energy peak (closed circles) also decreases towards the edge of the sample, but is not present on the side of the sample.

Fig. 2 shows the accumulated ion energy distribution (IED) for a typical point on the top of the stage (r = 1.6 cm). The accumulated IED tells us the history of the impinging ions at that position. Before the pulse is applied, ions deposit on to the sample with low energy. This *pre-pulse* peak in the accumulated IED appears in Fig. 2 at 0 keV. When the matrix sheath is formed, the ions in the matrix sheath implant with increasing energy while the

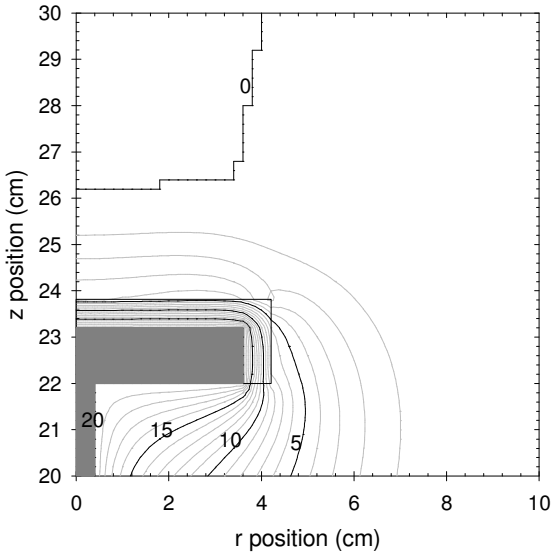

Fig.4 A contour plot of the electrostatic potential 1 μs after a −20 kV pulse has been switched on, numbers denote the potential in −kV. It can be seen at the top edge of the sample that the contour lines dip into the insulator, indicating that the magnitude of the electrostatic potential at the edge of the insulator is less than at other positions on the sample.

surface charge builds. Once the surface charge is large enough to repel the incoming ions, the ion energy ceases to rise before it then falls. This pause at a high energy causes a small peak in Fig. 2 at 19 keV. The ion energy then falls until it reaches its final resting value at 3.5 keV.

The pre-pulse peak, which is present at all positions along the sample, remains at approximately 0 keV. However, the location of the other two peaks varies with position along the sample. In Fig. 3, the location of the two higher energy peaks is plotted against position across the top, and then down the side of the sample. There is a clear decrease in the energy of the implanting ions near the edge of the sample (4.2 cm).

Fig. 4 shows the equipotentials 1 μs after the pulse has been switched on, i.e. at the same time as Fig. 1a. It can be seen that the equipotentials in the dielectric curve around the edge between the top and the side sections. The potential in the corner is around −3 kV, whereas the potential at other points along the top of the stage are approximately −5 kV. This is due to the insulator being thicker near the edge than it is elsewhere, thus the capacitive effects of the dielectric are more significant there. The edge effects of the insulator cause the decrease in ion energies near this location as was seen in Fig. 3.

The angle-energy plot (Fig. 5) tells the history of the ion energy on the vertical axis, while simultaneously tells the history of the ion implantation angle along the horizontal axis. The plot shown in Fig. 5 is for the point on the edge between the top and the side of the sample. Before the pulse is applied, ions impinge with a low energy (~0 keV) and at a slightly outward (negative) angle of incidence due to incident beam diffusion. Ions from within the matrix sheath implant with increasing energy in an inwardly (positive) direction until the surface charge has built up sufficiently that the sheath begins collapsing. During sheath collapse, implantation energy decreases and incident angle goes negative due to the concave sheath shape.

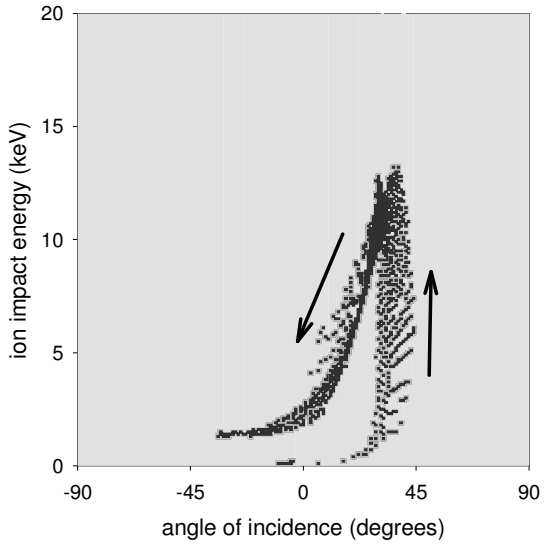

Fig.5 The angle-energy plot of the ions implanted on the outer edge of the sample shows a hysteresis. A positive angle of incidence means that ions are implanting from the (positive-r, positive-z)-quadrant.

4. Conclusion

In this study of plasma-immersion ion implantation of an insulating cap on a conducting stage, we have modeled the ion sheath collapse. We have shown that the sheath collapses at different rates across the surface. This variation in collapse rate affects the sheath shape and thus the dose distribution, ion implantation energy and angle. In particular, the ion energy has been shown to decrease near an insulating corner due to the thicker insulator size. The ion energy distribution is more strongly affected near the edges of the insulator.

[1] M. M. M. Bilek *et al.*, Contrib. Plasma Phys. **44**, 465 (2004).
[2] Y. Kim *et al.*, Surf. and Coat. Tech. **200**, 4763 (2006).
[3] Y. Y. Chang and D. Y. Wang, Surf. and Coat. Tech. **200**, 2187 (2005).
[4] P. K. Chu *et al.*, Material Sci. and Eng. R: Reports **36**, 143 (2002)
[5] N. Nosworthy *et al.*, Acta Biomaterialia **3**, 695 (2007).
[6] A. Anders, Vacuum **67**, 673 (2002).
[7] T. W. H. Oates *et al.*, IEEE Trans. Plasma Sci. **31**, 438 (2003).
[8] X. B. Tian *et al.*, Nucl. Instr. and Meth. in Phys. Res. B **187**, 485 (2002).
[9] X. B. Tian *et al.*, IEEE Trans. Plasma Sci. **32**, 792 (2004).
[10] X. B. Tian *et al.*, Surf. and Coat. Tech. **196**, 162 (2005).
[11] C. Cornet *et al.*, J. Applied Phys. **96**, 6045 (2004).
[12] C. K. Birdsall, *Plasma physics via computer simulation,* (CRC Press, 2005).
[13] G. A. Emmert and M. A. Henry, J. Applied Phys. **71**, 113 (1992).